PHOTONICS Research

Effects of the slot width and angular position on the mode splitting in slotted optical microdisk resonator

Lingling Dai,[1,2] Yiheng Yin,[1] Yanhui Hu,[1,2] Biyao Yang,[1] and Ming Ding[1,2,*]

[1]School of Instrument Science and Opto-Electronics Engineering, Beihang University, Beijing 100191, China
[2]International Research Institute for Multidisciplinary Science, Beihang University, Beijing 100191, China
*Corresponding author: mingding@buaa.edu.cn

Received 19 January 2017; revised 11 March 2017; accepted 11 March 2017; posted 15 March 2017 (Doc. ID 285239); published 17 April 2017

A novel slotted optical microdisk resonator, which significantly enhances light–matter interaction and provides a promising approach for increasing the sensitivity of sensors, is theoretically and numerically investigated. In this slotted resonator, the mode splitting is generated due to reflection of the slot. Remarkably, effects of the slot width and angular position on the mode splitting are mainly studied. The results reveal that the mode splitting is a second function of the slot width, and the maximum mode splitting induced by the slot deformation is achieved with 2.7853×10^9 Hz/nm. Therefore, the slotted resonator is an excellent candidate for pressure and force sensing. Besides, the influence of the slot angular position on the mode splitting is a cosine curve with the highest sensitivity of 1.23×10^{11} Hz/deg; thus, the optical characteristic demonstrates that the slotted resonator can be used for inertial measurements.

OCIS codes: (230.5750) Resonators; (230.0230) Optical devices; (060.2340) Fiber optics components; (060.2310) Fiber optics; (060.0060) Fiber optics and optical communications.

https://doi.org/10.1364/PRJ.5.000194

1. INTRODUCTION

In recent years, optical whispering gallery mode (WGM) resonators have attracted much attention owing to the small mode volume and the extreme high-quality factor (Q-factor) [1], which contribute to generating a considerable evanescent field and significantly enhancing the interaction between the light and matter [2]. In view of the mentioned advantages, optical WGM resonators provide an excellent platform for numerous practical applications, including low-threshold micro-lasers [3], narrow linewidth optical filters [4], cavity quantum electrodynamics [5], and sensors [6–8]. With the development of micro-nanofabrication technology, several WGM resonators with different designs, such as microdisks [9,10], microtoriods [11,12], and microspheres [13,14] as well as microbottles [15,16], have been theoretically and experimentally investigated.

In the optical WGM resonator, propagating modes are degenerate modes with the same polarization and resonant frequency along the circumference of resonator. Furthermore, there is the one-to-one correspondence between the azimuthal quantum number and the resonant frequency. However, propagating modes could be transformed into two non-degenerate eigenmodes as a result of the Rayleigh scattering when the subwavelength scatterers exist around the resonator. In the transmission spectrum, each azimuthal quantum number simultaneously corresponds to two resonant frequencies of non-degenerate eigenmodes. This phenomenon is called mode splitting and has been demonstrated to perform biosensing [13,17–21] by detecting the difference between the resonant frequencies of two eigenmodes rather than the shift of a single resonant frequency. Therefore, the sensors based on mode splitting offer robustness against noise such as an unstable light source and environmental disturbance. Researchers subsequently propose an active optical WGM resonator by doping the active medium to increase the sensitivity of sensors [22–24]. Nonetheless, only a portion of the evanescent field outside of the resonator interacts with matters because most of the light is constrained within the resonator as a result of total reflection, as illustrated in Fig. 1(a). Furthermore, the optical characteristic prevents further improvement to the sensor's sensitivity. To improve sensitivity, a novel slotted resonator is proposed by Aveline *et al.* [25]. Additionally, the nanoparticle detection is also demonstrated based on the slotted ring resonator [26]. In the slotted resonator, a strong peak of the localized electric field instead of a weak evanescent field can be accessed, as shown in Fig. 1(b). Although the working mechanism and the applications have been studied, effects of the slot width and angular position on the mode splitting are still not clear, which limits its versatility in multidisciplinary applications.

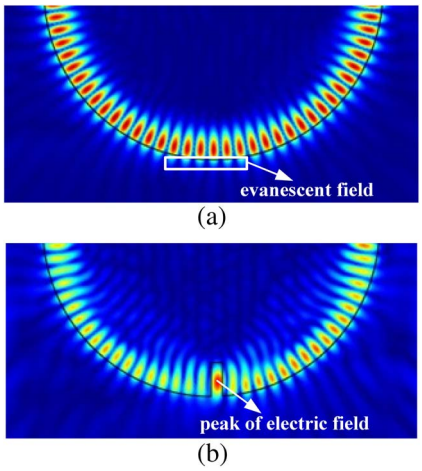

Fig. 1. (a) Electric field distribution of resonator. (b) Electric field distribution of the slotted resonator.

In this paper, a theoretical model for investigating impacts of the slot on the mode splitting is first developed. According to the model, the characteristics of transmission spectrum, including the strength of mode splitting, Q factor, and linewidth broadening dependence on the slot width and angular position, are discussed by theoretical calculations and numerical simulations. The results show that such a resonator has great potential in the pressure/force sensing and inertial measuring.

2. THEORY MODEL

The schematic of a coupled system is shown in Fig. 2. A 2D microdisk resonator with a refractive index of 1.4449 at the wavelength $\lambda = 1475.8$ nm and a diameter of 15 μm is analyzed throughout this work. For the coupled system, a tapered fiber with identical material to the resonator is applied to couple the evanescent light into and out of the resonator with the coupling rate κ_{ex}. The diameter of tapered fiber is 2 μm. In this paper, the gap between the tapered fiber and the slotted optical microdisk resonator is set to zero. On the edge of the resonator with the intrinsic loss rate κ_0, a slot with the slot depth of 700 nm and width of a is created, which induces an additional loss rate Γ. The angular position of a slot is described by the angle θ between the negative y axis and a straight line connecting the origin and the center of slot. In the counterclockwise (CCW) direction, θ is a positive value, on the contrary, θ is a negative value. Owing to the slot, a partial light reflects on the slot surfaces, and two non-degenerate WGMs with the cross-coupling rate γ_c are obtained. Finally, two standing wave modes (symmetric mode, SM; asymmetric mode, ASM) stably exist inside the slotted resonator due to the interference of the clockwise (CW) mode and CCW mode. The forward output light $a_{CW}^{out} = a_{in} + \sqrt{\kappa_{ex}} a_{CW}$ and backward output light $a_{CCW}^{out} = \sqrt{\kappa_{ex}} a_{CCW}$ are obtained through the tapered fiber.

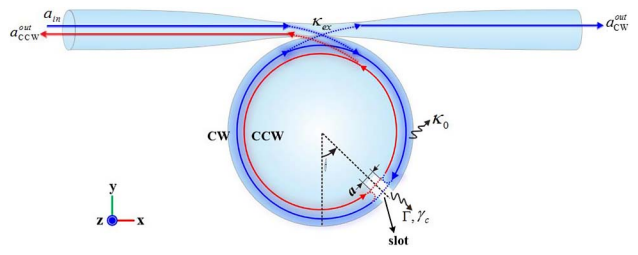

Fig. 2. Schematic of the optical WGM microdisk resonator with a single slot. a_{in}, the amplitude of input light; a_{CW}^{out}, output amplitude of CW; a_{CCW}^{out}, output amplitude of CCW.

The transmission of the coupled system can be written by the coupled mode theory [27]:

$$T = |a_{CW}^{out}|^2/|a_{in}|^2 = \left| 1 - \frac{\kappa_{ex}\left(-i\Delta w + i\gamma_c + \frac{\Gamma+\kappa_0+\kappa_{ex}}{2}\right)}{\left(-i\Delta w + i\gamma_c + \frac{\Gamma+\kappa_0+\kappa_{ex}}{2}\right)^2 - \left(i\gamma_c + \frac{\Gamma}{2}\right)^2} \right|^2, \quad (1)$$

where $\Delta w = w - w_c$ is illustrated as the detuning angular frequency between the excitation angular frequency w and the resonant angular frequency w_c.

Equation (1) shows that two resonant dips could be yielded in the transmission spectrum as $|2\gamma_c| > \kappa_0 + \kappa_{ex} + \Gamma$. The detuning frequency $\delta = \gamma_c/\pi$ between two resonant dips can be quantified by the cross-coupling rate γ_c, which represents the strength of mode splitting influenced by the slot width and angular position. Due to the lesser effect of slot depth on the mode splitting, the dependence of slot width and angular position on optical properties are mainly considered in the following sections.

A. Mode Splitting Dependence on the Slot Width

To simplify the proposed structure, the slot in the slotted resonator is regarded as a reflecting film with the reflectivity R [25]. Assuming that the incident light is perpendicular to the slot surface, the reflectivity of a slot could be calculated:

$$R = \frac{n-1}{n+1}\left[1 - \frac{4ne^{2ika}}{(n+1)^2 - e^{2ika}(n-1)^2}\right], \quad (2)$$

where n and a represent the refractive index of the slotted resonator and the slot width, respectively. The wavenumber k in the free space can be expressed as $k = 2\pi/\lambda$.

For the slotted resonator, the cross-coupling rate γ_c represents the proportion of counterpropagating resonant light per round-trip inside the optical resonator. Therefore, γ_c is strongly relevant to the reflectivity. In the ideal system without loss, γ_c can be described by $\gamma_c = |R|/\tau_0$. However, in the resonator coupled system, the loss rates, including the intrinsic loss rate κ_0, the coupling rate κ_{ex}, and the additional loss rate Γ, have an influence on the counterpropagating resonant light. The expression of γ_c can be rewritten as

$$\gamma_c = \frac{|R|}{\tau_0} - \gamma, \quad (3)$$

where $\tau_0 = 2\pi n R_0/c$ is the optical round-trip time in the resonator with radius R_0. $\gamma = (\kappa_0 + \kappa_{ex} + \Gamma)/2$ describes the total loss rate of the coupled system, in which the coupling rate κ_{ex} could be regarded as a constant due to the lesser impact of width variation on the coupling rate κ_{ex} compared with the module reflectivity $|R|$ and the additional loss rate Γ. In analogy to Eq. (3), Γ can be described as

$$\Gamma = \frac{\Gamma_s}{\tau_0} = \frac{\int_{\delta S} n^2(\boldsymbol{r})|\boldsymbol{E}(\boldsymbol{r})|^2 \mathrm{d}\boldsymbol{r}}{\tau_0 \int n^2(\boldsymbol{r})|\boldsymbol{E}^0(\boldsymbol{r})|^2 \mathrm{d}\boldsymbol{r}}, \tag{4}$$

where δS indicates the region of the slot. The value of the integral area is decided by the width and the angular position of the slot. Γ_s represents the fraction of energy within the slot. $n(\boldsymbol{r})$ and $\boldsymbol{E}^0(\boldsymbol{r})$ are the refractive index and the distribution of unperturbed electric field in the resonator, respectively. $\boldsymbol{E}(\boldsymbol{r})$ describes the electric field in the slot.

For the microdisk in two dimensions, the distributions of the electric field in the radial and angular direction are established by Maxwell's equations:

$$\begin{cases} E_\rho = \frac{j}{w^2\mu_0\varepsilon_i - \beta^2}\left(\beta \frac{\mathrm{d}E_z}{\mathrm{d}\varphi} - \frac{jm w\mu_0}{\rho} H_z\right) \\ E_\varphi = \frac{j}{w^2\mu_0\varepsilon_i - \beta^2}\left(\frac{jm\beta}{\rho} E_z + w\mu_0 \frac{\mathrm{d}H_z}{\mathrm{d}\rho}\right) \\ H_\rho = \frac{j}{w^2\mu_0\varepsilon_i - \beta^2}\left(\beta \frac{\mathrm{d}H_z}{\mathrm{d}\varphi} + \frac{jmw\varepsilon_i}{\rho} E_z\right) \\ H_\varphi = \frac{j}{w^2\mu_0\varepsilon_i - \beta^2}\left(\frac{jm\beta}{\rho} H_z - w\varepsilon_i \frac{\mathrm{d}E_z}{\mathrm{d}\rho}\right) \end{cases}, \tag{5}$$

where m, w, μ_0, ε_i, and β illustrate the azimuthal quantum number, angular frequency, permeability of free space, permittivity, and propagating constant, respectively.

The electric field E_z and the magnetic field H_z in the z direction can be characterized by the product of two functions, $E_z(H_z) = \Psi(\rho)\Upsilon(\varphi)$. $\Psi(\rho)$ only depends on the radius ρ from the center of the microdisk resonator and can be written as

$$\Psi(\rho) = \begin{cases} A_m J_m(k_0 n_{\mathrm{eff}}\rho), & \rho \le R_0 \\ B_m H_m^{(1)}(k_0\rho), & \rho > R_0 \end{cases}, \tag{6}$$

where R_0 and n_{eff} are the microdisk radius and the effective refractive index inside the resonator. A_m and B_m indicate the normalized parameters determined by the boundary conditions of the electromagnetic field. $\Upsilon(\varphi)$ is a function of the polar angle φ and can be illustrated as $\Upsilon(\varphi) \sim e^{\pm jm\varphi}$.

Combined with the Eqs. (2)–(6), the cross-coupling rate γ_c can be rewritten as

$$\gamma_c = \left|\frac{n-1}{\tau_0(n+1)}\left[1 - \frac{4ne^{2ika}}{(n+1)^2 - e^{2ika}(n-1)^2}\right]\right| - \left[\kappa_0 + \kappa_{\mathrm{ex}} + \frac{\int_{\delta S} n^2(\boldsymbol{r})|\boldsymbol{E}(\boldsymbol{r})|^2 \mathrm{d}\boldsymbol{r}}{\int n^2(\boldsymbol{r})|\boldsymbol{E}(\boldsymbol{r})|^2 \mathrm{d}\boldsymbol{r}}\right]/2. \tag{7}$$

And then the detuning frequency $\delta = \gamma_c/\pi$ is calculated. Equation (7) shows that γ_c is determined by the slot width a. Therefore, the mode splitting has a dependence on the slot width.

B. Mode Splitting Dependence on the Slot Angular Position

In the theory model, the slot also could be interpreted as a perturbation when the slot size is much smaller than the wavelength ($<\lambda/4$). Therefore, the perturbation theory can be applied to predict the resonant frequency shift of the split mode Δf_θ caused by the angular position variation of slot [28]:

$$\Delta f_\theta = -\frac{f^0}{2}\frac{\langle \boldsymbol{E}_{\mathrm{CW}}|\Delta\varepsilon|\boldsymbol{E}_{\mathrm{CCW}}\rangle}{\langle \boldsymbol{E}^0|\varepsilon^0|\boldsymbol{E}^0\rangle} + (\Gamma + \kappa_{\mathrm{ex}} + \kappa_0)/4\pi, \tag{8}$$

where θ, ε^0, f^0, $\boldsymbol{E}^0$ represent the slot angular position, medium permittivity, unperturbed resonant frequency, and the electric field without the slot, respectively. $\boldsymbol{E}_{\mathrm{CW}}$ and $\boldsymbol{E}_{\mathrm{CCW}}$ describe the electric field distribution in the CS and anticlockwise directions. In the Eq. (8), we can conclude that the parameters of the intrinsic loss rate κ_0, the additional loss rate Γ, and the coupling loss rate κ_{ex} have an influence on Δf_θ. The shift of resonant frequency is related with the variation value of γ_c. Therefore, γ_c can be quantified by Δf_θ. The perturbation $\Delta\varepsilon$ can be written as $\Delta\varepsilon = \varepsilon^0\delta n^2\Delta r(\varphi)\delta(r - R_0)$, where $\delta n^2 = n_r^2 - n_0^2$, n_r represents the refractive index of resonator, and n_0 is the refractive index of the surrounding medium. $\Delta r(\varphi)$ describes the difference between the slotted resonator radius, which depends on the polar angle φ, and the unperturbed resonator radius R_0, as illustrated in Fig. 3. $\delta(r - R_0)$ is an impulse function, whose value equals 1 as $r = R_0$. In the Eq. (8), the denominator of the first term denotes the time-averaged stored energy inside the resonator, and the numerator describes the energy within the slot varied with the slot angular position. The Dirac notation is used for the inner product computation $\langle \boldsymbol{E}^0|\boldsymbol{E}^0\rangle = \int \boldsymbol{E}^0(\boldsymbol{r})[\boldsymbol{E}^0(\boldsymbol{r})]^* \mathrm{d}\boldsymbol{r}$. Then the Eq. (8) can be rewritten as

$$\Delta f_\theta = -\frac{f^0 \int \Delta\varepsilon(\boldsymbol{r})\boldsymbol{E}_{\mathrm{CW}}(\boldsymbol{r})\boldsymbol{E}^*_{\mathrm{CCW}}(\boldsymbol{r})\mathrm{d}\boldsymbol{r}}{2\int \varepsilon^0(\boldsymbol{r})|\boldsymbol{E}^0(\boldsymbol{r})|^2 \mathrm{d}\boldsymbol{r}} + (\Gamma + \kappa_{\mathrm{ex}} + \kappa_0)/4\pi. \tag{9}$$

As mentioned above, the integral area of Eq. (4) depends on the angular position of slot. Thus, the additional loss rate Γ is closely related with the angular position of the slot. In the tapered fiber-slotted resonator coupled system, the coupling rate κ_{ex} only depends on the gap between the tapered fiber and the resonator when the slot is far away from the tapered fiber. However, the angular position has an effect on the coupling rate κ_{ex} when the slot is located nearby the tapered fiber. The reason is that a part of coupling light is reflected on the slot surfaces and coupled into the tapered fiber or dissipated. Because the expression of coupling rate is more complicated and the lesser effect of angular position variation on the coupling rate κ_{ex}, we consider that κ_{ex} is only a function of the gap between the tapered fiber and the resonator in the theoretical model for simplifying the model:

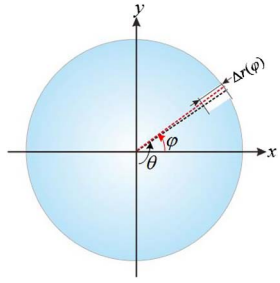

Fig. 3. Schematic representation of $\Delta r(\varphi)$, φ, and θ are the polar angle and the angular position of slot, respectively.

$$\kappa_{ex} = \frac{k}{4}\sqrt{\frac{\varepsilon_0}{\mu_0}}\int \delta n^2(\boldsymbol{r})\boldsymbol{E}^0(\boldsymbol{r})\boldsymbol{E}_{fiber}(\boldsymbol{r})\mathrm{d}\boldsymbol{r}, \quad (10)$$

where $\delta n^2(\boldsymbol{r})$ represents the refractive index difference between the resonator and the surrounding medium. $\boldsymbol{E}_{fiber}(\boldsymbol{r})$ expresses the electric field of the tapered fiber.

According to the Eqs. (9) and (10), the shift of mode splitting, which exhibits a strong dependence on the angular position, can be calculated. Consequently, the detection of slot angular position is realized by measuring the mode splitting shift. For the inertial measurement system, the angular position is an important parameter to determine the attitude information of aircraft. Therefore, our approach can be used for inertial measurements and to support a simpler detection process compared with the traditional inertial devices.

3. RESULTS AND DISCUSSIONS

To further investigate the effects of a slot on the mode splitting, the numerical simulation is carried out using the finite element method (FEM). The model is defined and studied by the commercial software COMSOL 5.2 Multiphysics. The chosen boundary conditions are the continuity and scattering boundary conditions as the interior and exterior boundaries and the port boundary at the input and output surfaces. Simulations are run with controlled mesh size (150 nm in air and 100 in silica) to make efficient use of computer memory. Figure 4 plots the normalized transmission in a slotted resonator with the slot width 220 nm and the slot angular position 0°. The normalized detuning frequency $\delta_N(\delta_N = \delta/\kappa_0, \kappa_0 = 1.211 \times 10^{11}$ Hz) represents the amount of mode splitting. In Fig. 4, the doublet transmission dips corresponding to mutually orthogonal standing waves SM and ASM are observed. The theoretical fitting curve (the red solid line) calculated by Eqs. (1)–(3) is in accordance with the simulation result (the blue dot–dash line). In the slotted resonator, the resonant wavelength can be approximately described by $2\pi n_{eff}R_0 = m\lambda$, where n_{eff} and m represent the effective index refractive and the azimuthal number at the resonant wavelength, respectively. The resonant wavelength of SM experiences a significant blueshift with respect to the unperturbed ASM, for which the existence of a slot leads to the decrease of effective index in the slotted resonator.

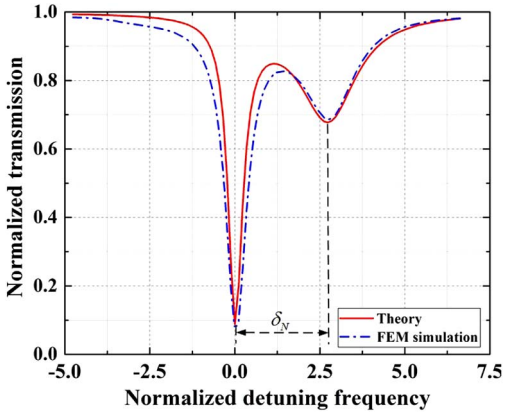

Fig. 4. Normalized transmission of the theory model (red solid line) and FEM simulation (blue dash–dot line) with the slot width of 220 nm and the slot angular position of 0°. The close agreement between the theoretical and simulation result is obtained with $\kappa_0 = 1.211 \times 10^{11}$ Hz, $\Gamma = 1.65\kappa_0$, $\kappa_{ex} = 1.78\ \kappa_0$, $\gamma = 2.215\kappa_0$, and $\gamma_c = 8.4\kappa_0$.

A. Mode Splitting Dependence on the Slot Width

In the following section, the influence of slot width on the mode splitting is discussed. Figure 5 shows the normalized transmission spectra in the absence of the slot and with different slot widths. Due to the existence of the slot, the resonant dip of ASM becomes shallow. However, the linewidth of ASM is almost unchanged with the increase of slot width because the ASM locates the slot at the node of the electric field. Conversely, the linewidth of SM is broadened, which indicates that the SM locates the slot at the anti-node of the electric field.

In the slotted resonator with a narrower slot, the intensity of the backward reflected light is weakening and gives rise to a decrease in the cross-coupling intensity between the forward light and the backward reflected light. Furthermore, the weak cross-coupling is unable to provide enough intensity for generating stably resonant light in a CCW direction. Consequently, the transmission dip of SM becomes shallow with the decrease of slot width and disappears with a smaller width of 50 nm, as shown in Fig. 5. The minimum slot width needed to generate mode splitting is inversely proportional to the cross-coupling rate γ_c. According to Eq. (3), γ_c is increasing with the decrement of intrinsic κ_0 loss rate determined by the ratio of the resonant angular frequency w_c and the intrinsic quality factor Q_0. Therefore, the minimum slot width needed to generate mode splitting can be diminished in a resonator with high Q factor, such as the active resonator.

In Fig. 6(a), the normalized detuning frequencies under different widths are obtained by FEM simulation, and the fitting curve (red dash line) can be represented by the quadratic

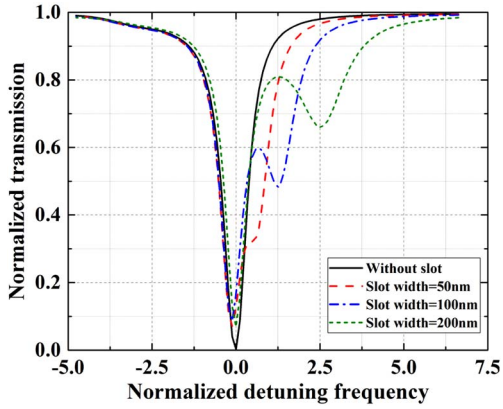

Fig. 5. Simulation results of the normalized transmission without single slot (corresponding parameter in the theoretical model: $\kappa_0 = 1.211 \times 10^{11}$ Hz, $\kappa_{ex} = 1.78\kappa_0$) and under the difference slot width of 50 nm (corresponding parameters in the theoretical model: $\kappa_0 = 1.211 \times 10^{11}$ Hz, $\Gamma = 0.4\kappa_0$, $\kappa_{ex} = 1.78\kappa_0$, $\gamma = 1.59\kappa_0$ and $\gamma_c = 1.4\kappa_0$), 100 nm (corresponding parameters in the theoretical model: $\kappa_0 = 1.211 \times 10^{11}$ Hz, $\Gamma = 0.7\kappa_0$, $\kappa_{ex} = 1.78\kappa_0$, $\gamma = 1.74\kappa_0$ and $\gamma_c = 3.9\kappa_0$) and 200 nm (corresponding parameters in the theoretical model: $\kappa_0 = 1.211 \times 10^{11}$ Hz, $\Gamma = 1.4\kappa_0$, $\kappa_{ex} = 1.78\kappa_0$, $\gamma = 2.09\kappa_0$ and $\gamma_c = 7.9\kappa_0$).

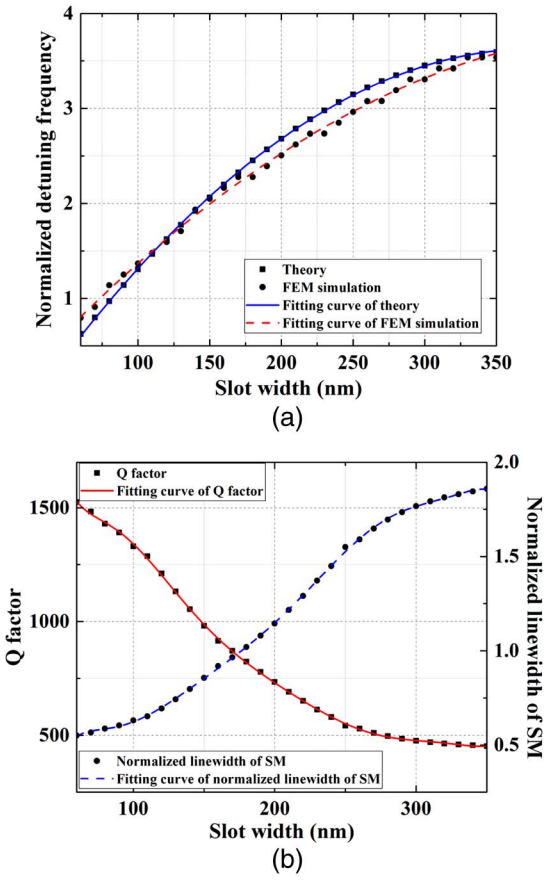

Fig. 6. (a) Normalized detuning frequency as a function of the slot width; the blue solid curve presents the theoretical results, and the red dash curve depicts the simulation results. (b) Normalized linewidth broadening induced by the slot and Q factor of the slotted resonator with different slot widths.

function $-1.819 \times 10^{-5}a^2 + 0.01703a - 0.1515$. The theoretical result (blue solid line) calculated by Eq. (3) shows close agreement with the simulation as theoretical parameters $\kappa_0 = 1.211 \times 10^{11}$ Hz and $\kappa_{ex} = 1.78\kappa_0$. The explanation of the slight difference between the simulation and theory is in the theory model. We assume that the incident light is perpendicular to the slot surface; however, the incident angle depends on the slot location and the propagating path of light in the simulation analysis. Figure 6(a) shows that the growth rate of the normalized detuning frequency is decreased with the increase of slot width, and the maximum mode splitting resulting from the slot deformation is approximately 2.7853×10^9 Hz/nm at the slot width ~150 nm. The characteristics demonstrate that the coupled system is feasible for measuring parameters, which induces the variation of slot width, such as pressure and force. In Fig. 6(b), the variation of slot width has a negative effect on the Q factor, which is dropped down to only 500 as the slot width of 350 nm. As we all know, the Purcell factor is proportional to the Q factor of a resonator. Therefore, the mode splitting is unable to generate when the slot width is larger than a quarter wavelength because of the low Q factor. Besides, Fig. 6(b) shows that the SM linewidth, which is inversely proportional to the Q factor, goes up with the increase of slot width.

B. Mode Splitting Dependence on the Slot Angular Position

Equations (8)–(10) predict that the mode splitting displays a correlation with the slot angular position. As depicted in Fig. 7(a), the linewidth is affected by the slot angular position. The phenomenon indicates that the Q factor is a function of the angular position. In Fig. 7(b), the growth rate of the normalized detuning frequency is also varied with the angular position. The minimum slot widths needed to generate mode splitting are different owing to the variation of the Q factor with different slot angular positions.

Figure 8 represents the normalized detuning frequencies under different slot angular positions performed by the FEM simulation and theoretical model for the case of azimuthal number $m = 41$. The theoretical result displays good

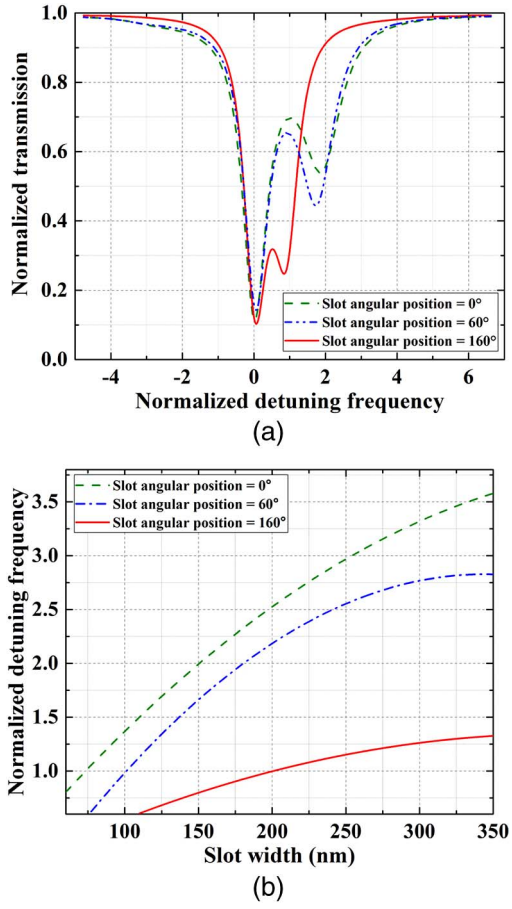

Fig. 7. (a) Normalized transmission in a slotted resonator with the slot width of 150 nm and the slot angular position of 0° (corresponding parameters in the theoretical model: $\kappa_0 = 1.211 \times 10^{11}$ Hz, $\Gamma = \kappa_0$, $\kappa_{ex} = 1.78\kappa_0$, $\gamma = 1.89\kappa_0$, and $\gamma_c = 6.1\kappa_0$), 60° (corresponding parameters in the theoretical model: $\kappa_0 = 1.211 \times 10^{11}$ Hz, $\Gamma = 0.85\kappa_0$, $\kappa_{ex} = 1.78\kappa_0$, $\gamma = 1.815\kappa_0$, and $\gamma_c = 5.8\kappa_0$) and 160° (corresponding parameters in the theoretical model: $\kappa_0 = 1.211 \times 10^{11}$ Hz, $\Gamma = 0.6\kappa_0$, $\kappa_{ex} = 2\kappa_0$, $\gamma = 1.8\kappa_0$, and $\gamma_c = 3.3\kappa_0$). (b) Relationship between slot width and normalized detuning frequency with the slot angular position of 0° (green dash line), 60° (blue dash–dot line), and 160° (red solid line).

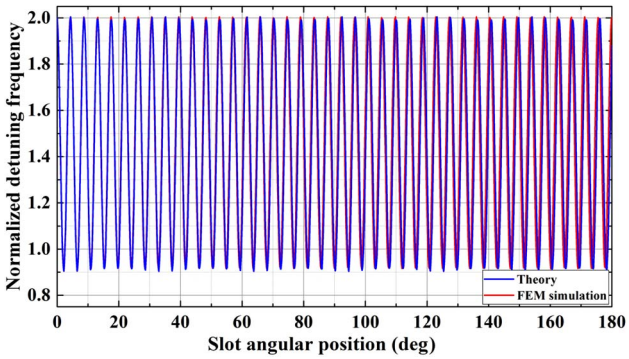

Fig. 8. Normalized detuning frequency as a function of the slot angular position in a slotted resonator with the slot width of 150 nm. Blue line presents the theory analysis results; red line depicts the FEM simulation results for the case of azimuthal number $m = 41$.

agreement with the simulation when the slot angular position is far away from the tapered fiber. However, a slight mismatch with the simulation result gradually emerges when the slot is located near the tapered fiber, which is due to a part of the reflected light escaping from the slot and coupling into the tapered fiber in the FEM simulation.

In the resonator, the intensity distribution of the electric field is periodic on the circle, and the number of cycles is described by the azimuthal number m. Existence of the slot results in a perturbation on the electric field intensity, which leads to the mode splitting generation in transmission spectrum. Therefore, the mode splitting is closely related to the perturbation, which has dependence on the electric field intensity in the corresponding slot angular position. As shown in Fig. 8, the maximum mode splitting, which represents the strongest influence of a slot on the electric field, is achieved when the slot is located on the peak of the electric field intensity. Similarly, the minimum value appears on the wave troughs of the intensity. As a consequence, the mode splitting experiences a periodic oscillation with the period approximately 4.4° and the number of cycles m. The characteristic provides a broad stage on the angular position detection with the maximum calculated sensitivity 1.23×10^{11} Hz/deg. The accuracy of measurement could be improved by monitoring numerous resonant modes or modifying the slotted resonator for breaking the periodicity, such as fabricating an asymmetry slotted resonator and increasing the number of slots.

4. CONCLUSION

In conclusion, a theoretical model of the slotted resonator is investigated, and FEM simulations are carried out to verify the model. In the slotted resonator, strong mode splitting is observed because two counterpropagating resonant modes stably exist as a result of the reflection. The effects of slot width and angular position on the mode splitting are numerically studied by perturbation theory and FEM simulation. The calculation reveals that the maximum sensitivity with respect to the width variation is approximately 2.78×10^9 Hz/nm. The existence of slot results in the decrement of the Q factor, and the value diminishes with expanding the slot width. Additionally, the cosine relationship between the mode splitting and angular position is obtained with an ultrahigh sensitivity of $\sim 1.23 \times 10^{11}$ Hz/deg. Compared with the conventional resonator, the sensitivity of the slotted resonator could be improved because a strong peak field, rather than the weak evanescent field, overlaps with matter. The presented research of the slotted resonator displays great potential in the pressure measurement and inertial sensing.

Funding. National Natural Science Foundation of China (NSFC) (61575014); Natural Science Foundation of Beijing Municipality (4162038).

REFERENCES

1. A. B. Matsko and V. S. Ilchenko, "Optical resonators with whispering-gallery modes-part I: basics," IEEE J. Sel. Top. Quantum Electron. **12**, 15–32 (2013).
2. K. J. Vahala, "Optical microcavities," Nature **424**, 839–846 (2015).
3. S. M. Spillane, T. J. Kippenberg, and K. J. Vahala, "Ultralow-threshold Raman laser using a spherical dielectric microcavity," Nature **415**, 621–623 (2002).
4. H. Rokhsari and K. J. Vahala, "Ultralow loss, high Q, four port resonant couplers for quantum optics and photonics," Phys. Rev. Lett. **92**, 253905 (2004).
5. T. Aoki, B. Dayan, E. Wilcut, W. P. Bowen, A. S. Parkins, T. J. Kippenberg, K. J. Vahala, and H. J. Kimble, "Observation of strong coupling between one atom and a monolithic microresonator," Nature **443**, 671–674 (2006).
6. J. Chaste, A. Eichler, J. Moser, G. Ceballos, R. Rurali, and A. Bachtold, "A nanomechanical mass sensor with yoctogram resolution," Nat. Nanotechnol. **7**, 301–304 (2012).
7. A. R. Ali, T. Ioppolo, V. Ötügen, M. Christensen, and D. MacFarlane, "Photonic electric field sensor based on polymeric microspheres," J. Polym. Sci. B **52**, 276–279 (2014).
8. F. Vollmer and L. Yang, "Review label-free detection with high-Q microcavities: a review of biosensing mechanisms for integrated devices," Nanophotonics **1**, 267–291 (2012).
9. A. M. Armani, R. P. Kulkarni, and S. E. Fraser, "Label-free, single-molecule detection with optical micro-cavities," Science **317**, 783–787 (2007).
10. S. M. Grist, S. A. Schmidt, and J. Flueckiger, "Silicon photonic micro-disk resonators for label-free biosensing," Opt. Express **21**, 7994–8006 (2013).
11. T. J. Kippenberg, S. M. Spillane, and K. J. Vahala, "Demonstration of ultra-high-Q small mode volume toroid microcavities on a chip," Appl. Phys. Lett. **85**, 6113–6115 (2004).
12. D. K. Armani, T. J. Kippenberg, S. M. Spillane, and K. J. Vahala, "Ultra-high-Q toroid microcavity on a chip," Nature **421**, 925–928 (2003).
13. M. L. Gorodetsky, A. D. Pryamikov, and V. S. Ilchenko, "Rayleigh scattering in high-Q microspheres," J. Opt. Soc. Am. B **17**, 1051–1057 (2000).
14. D. Farnesi, A. Barucci, and G. C. Righini, "Optical frequency conversion in silica-whispering-gallery-mode microspherical resonators," Phys. Rev. Lett. **112**, 093901 (2014).
15. D. O'Shea, A. Rettenmaier, and A. Rauschenbeutel, "Active frequency stabilization of an ultra-high Q whispering-gallery-mode microresonator," Appl. Phys. B **99**, 623–627 (2010).
16. C. Junge, S. Nickel, and D. O'Shea, "Bottle microresonator with actively stabilized evanescent coupling," Opt. Lett. **36**, 3488–3490 (2011).
17. D. S. Weiss, V. Sandoghdar, J. Hare, V. Lefevre-Seguin, J. M. Raimond, and S. Haroche, "Splitting of high-Q Mie modes induced by light backscattering in silica microspheres," Opt. Lett. **20**, 1835–1837 (1995).

18. J. Zhu, S. K. Özdemir, Y. F. Xiao, L. Li, L. He, D. R. Chen, and L. Yang, "On-chip single nanoparticle detection and sizing by mode splitting in an ultrahigh-Q microresonator," Nat. Photonics **4**, 46–49 (2009).
19. J. Wiersig, "Enhancing the sensitivity of frequency and energy splitting detection by using exceptional points: application to microcavity sensors for single-particle detection," Phys. Rev. Lett. **112**, 203901 (2014).
20. X. Yi, Y. F. Xiao, Y. C. Liu, B. B. Li, Y. L. Chen, Y. Li, and Q. H. Gong, "Multiple-Rayleigh-scatterer-induced mode splitting in a high-Q, whispering-gallery-mode microresonator," Phys. Rev. A **83**, 23803 (2011).
21. T. J. Kippenberg, "Microresonators: particle sizing by mode splitting," Nat. Photonics **4**, 9–10 (2010).
22. B. B. Li, W. R. Clements, X. C. Yu, K. B. Shi, Q. H. Gong, and Y. F. Xiao, "Single nanoparticle detection using split-mode microcavity Raman lasers," Proc. Natl. Acad. Sci. USA **111**, 14657–14662 (2014).
23. L. He, S. K. Özdemir, J. Zhu, and L. Yang, "Ultra-sensitive detection of mode splitting in active optical microcavities," Phys. Rev. A **82**, 053810 (2010).
24. L. He, S. K. Ozdemir, Y. F. Xiao, and L. Yang, "Gain-induced evolution of mode splitting spectra in a high-, active microresonator," IEEE J. Quantum Electron. **46**, 1626–1633 (2010).
25. D. C. Aveline, D. V. Strekalov, and N. Yu, "Micro-slotted whispering gallery mode resonators for optomechanical," Appl. Phys. Lett. **105**, 021111 (2014).
26. S. Wang, K. Broderick, and H. Smith, "Strong coupling between on chip notched ring resonator and nanoparticle," Appl. Phys. Lett. **97**, 051102 (2010).
27. A. Mazzei, S. Gotzinger, L. S. Menezes, G. Zumofen, O. Benson, and V. Sandoghdar, "Controlled coupling of counter propagating whispering-gallery modes by a single Rayleigh scatterer: a classical problem in a quantum optical light," Phys. Rev. Lett. **99**, 173603 (2007).
28. S. G. Johnson, M. Ibanescu, M. A. Skorobogatiy, O. Weisberg, J. D. Joannopoulos, and Y. Fink, "Perturbation theory for Maxwell's equations with shifting material boundaries," Phys. Rev. E **65**, 066611 (2002).